

Journal of Biomaterials Science, Polymer Edition

ISSN: 0920-5063 (Print) 1568-5624 (Online) Journal homepage: www.tandfonline.com/journals/tbsp20

Lecithin-chitosan nanoparticles for co-delivery of curcumin and β-caryophyllene—potential applications in chronic wound care

Lisa Myrseth Hemmingsen, Luca Boracchia, Nadia Eriksen Hagen, Terje Vasskog, Fabiola Guareschi, Fabio Sonvico & Nataša Škalko-Basnet

To cite this article: Lisa Myrseth Hemmingsen, Luca Boracchia, Nadia Eriksen Hagen, Terje Vasskog, Fabiola Guareschi, Fabio Sonvico & Nataša Škalko-Basnet (2026) Lecithin-chitosan nanoparticles for co-delivery of curcumin and β-caryophyllene—potential applications in chronic wound care, Journal of Biomaterials Science, Polymer Edition, 37:12, 2247-2271, DOI: 10.1080/09205063.2025.2582737

To link to this article: https://doi.org/10.1080/09205063.2025.2582737

© 2025 The Author(s). Published by Informa UK Limited, trading as Taylor & Francis Group

View supplementary material

Published online: 05 Nov 2025.

Submit your article to this journal

Article views: 1434

View related articles

View Crossmark data

Citing articles: 2 View citing articles

Full Terms & Conditions of access and use can be found at
https://www.tandfonline.com/action/journalInformation?journalCode=tbsp20

JOURNAL OF BIOMATERIALS SCIENCE, POLYMER EDITION
2026, VOL. 37, NO. 12, 2247–2271
https://doi.org/10.1080/09205063.2025.2582737

Taylor & Francis
Taylor & Francis Group

OPEN ACCESS Check for updates

Lecithin-chitosan nanoparticles for co-delivery of curcumin and β-caryophyllene—potential applications in chronic wound care

Lisa Myrseth Hemmingsen[a,b], Luca Boracchia[b,c*], Nadia Eriksen Hagen[a*], Terje Vasskog[a], Fabiola Guareschi[c], Fabio Sonvico[c] and Nataša Škalko-Basnet[b]

[a]Natural Products and Medicinal Chemistry Research Group, Department of Pharmacy, University of Tromsø, The Arctic University of Norway, Tromsø, Norway; [b]Drug Transport and Delivery Research Group, Department of Pharmacy, University of Tromsø, The Arctic University of Norway, Tromsø, Norway; [c]Department of Food and Drug Science, ADDRes–Advanced Drug Delivery Research Lab, Università di Parma, Parma, Italy

ABSTRACT

Chronic skin wounds pose a significant challenge due to persistent inflammation, elevated oxidative stress, and high susceptibility to microbial colonization. To support wound healing, this study investigated lecithin-chitosan nanoparticles co-loaded with curcumin and β-caryophyllene, two natural compounds with complementary anti-inflammatory, antioxidative, and antimicrobial properties. Co-loading curcumin and β-caryophyllene produced near-spherical nanoparticles with consistent size distribution (200–240 nm) and favourable surface charge (+30–35 mV) for topical applications. The *in vitro* release studies showed gradual, sustained curcumin release over 24 h, with encapsulation modestly affecting permeation. Furthermore, ABTS and DPPH assays revealed strong radical scavenging activity of curcumin, comparable to vitamin E and slightly lower than vitamin C, supporting its potential to mitigate oxidative damage in chronic wounds. Anti-inflammatory activity was confirmed *via* nitric oxide inhibition in lipopolysaccharide-induced murine macrophages, where co-loaded nanoparticles significantly reduced NO production in a concentration-dependent manner. Cytotoxicity testing showed that while free curcumin reduced cell viability, the encapsulated compound was notably non-toxic. The nanoparticles also demonstrated strong antimicrobial activity against *Staphylococcus aureus*, reducing bacterial growth to nearly zero in the co-loaded formulation. These findings highlight curcumin and β-caryophyllene co-loaded lecithin–chitosan nanoparticles as a promising platform for topical chronic wound treatment, offering dual delivery and synergistic effects against inflammation, oxidative stress, and infection. To our knowledge, this is the first study to co-deliver curcumin and β-caryophyllene in lecithin-chitosan nanoparticles, enabling a unified antioxidant, anti-inflammatory, and antimicrobial strategy for chronic wound therapy.

ARTICLE HISTORY
Received 15 September 2025
Accepted 24 October 2025

KEYWORDS
Chronic wounds; lecithin-chitosan nanoparticles; curcumin; β-caryophyllene; topical drug delivery; infection

CONTACT Lisa Myrseth Hemmingsen lisa.m.hemmingsen@uit.no Department of Pharmacy, University of Tromsø, The Arctic University of Norway, Universitetsvegen 57, Tromsø, 9037, Norway
*These authors contributed equally to this work.

Supplemental data for this article is available online at https://doi.org/10.1080/09205063.2025.2582737

© 2025 The Author(s). Published by Informa UK Limited, trading as Taylor & Francis Group
This is an Open Access article distributed under the terms of the Creative Commons Attribution-NonCommercial-NoDerivatives License (http://creativecommons.org/licenses/by-nc-nd/4.0/), which permits non-commercial re-use, distribution, and reproduction in any medium, provided the original work is properly cited, and is not altered, transformed, or built upon in any way. The terms on which this article has been published allow the posting of the Accepted Manuscript in a repository by the author(s) or with their consent.

GRAPHICAL ABSTRACT



1. Introduction

Chronic skin wounds, including diabetic foot ulcers, venous leg ulcers, and pressure ulcers, represent a major healthcare burden due to their prolonged healing times, high risk of infection, and related complications. Unlike acute wounds, chronic wounds fail to progress through the normal stages of healing, mainly due to persistent inflammation, elevated oxidative stress, and microbial colonization [1,2]. These factors disrupt cellular function, impair tissue regeneration, and create a hostile microenvironment that delays closure of the wounded area [3].

Efficient management of chronic wounds requires therapeutic approaches that target the complex physiological processes underlying impaired healing [4]. Inflammation is characterized by the excessive production of pro-inflammatory mediators such as nitric oxide, which contribute to tissue damage and prolonged inflammation. Simultaneously, oxidative stress from reactive oxygen species (ROS) increases cellular injury and further impedes repair mechanisms [5]. Additionally, bacterial colonization, often by *Staphylococcus aureus*, can lead to biofilm formation, increasing resistance to conventional antibiotics, and prolonged inflammation [6,7].

Natural compounds with anti-inflammatory, antioxidative, and antimicrobial properties are gaining attention as therapeutics in wound care [8]. Curcumin (CUR), a polyphenolic compound derived from *Curcuma longa*, exhibits both radical scavenging and anti-inflammatory activities; however, it suffers from poor aqueous solubility and stability, limiting its translation into the clinics [9–11]. Moreover, β-caryophyllene (βCAR), a sesquiterpene found in many essential oils, also possesses anti-inflammatory and antimicrobial effects [12,13]. Co-delivery of these compounds could provide complementary mechanisms to mitigate inflammation and infection [14] while promoting tissue repair. Combining CUR and βCAR into a single regimen introduces a novel strategy with the potential to unify antioxidative, anti-inflammatory, and antimicrobial actions within a single formulation for future chronic wound therapies.

Nanoparticle-based delivery systems have emerged as promising platforms to enhance the bioavailability, stability, and controlled release of hydrophobic therapeutic agents [15], characteristics that are particularly favourable for the compounds like CUR and βCAR. Lecithin-chitosan nanoparticles (LCNs) combine the bioactive and

bioadhesive properties of chitosan with the biocompatibility of lecithin to form stable carriers potentially able to control or sustain release and improve skin penetration [16–18]. The positive charge of chitosan could facilitate interaction with the negatively charged skin surface and microbial membranes, possibly enhancing both delivery and antimicrobial activity [19,20].

This study investigated the development and characterization of LCNs co-loaded with CUR and βCAR for potential topical application in chronic wound treatment. The physicochemical characterization, release behaviour, and evaluation of the antioxidative, anti-inflammatory, cytotoxic, and antimicrobial properties of the LCNs were focus points of this study. Together, these investigations aimed to determine the therapeutic potential of this multifunctional delivery system in addressing the challenges of chronic wounds and improve therapeutic outcome. This study is, to the best of our knowledge, the first to explore the synergistic incorporation of CUR and βCAR into LCNs.

2. Materials and methods

2.1. Materials

Chitopharm™ M-Chitosan with medium molecular weight (average of 350–600 kDa) and degree of deacetylation of >70% was kindly provided by Chitinor (Tromsø, Norway). Lipoid S45 was kindly supplied by Lipoid GmbH (Ludwigshafen, Germany). Pharmaceutical-grade oils Labrafac lipophile WL1349 (medium-chain triglycerides, EP) and Maisine® CC (glycerol 147 monolinoleate) from Gattefossé were kindly gifted by Azelis (Herlev, Denmark). β-caryophyllene (βCAR, ≥80%), curcumin (CUR, ≥94%), 2,2-diphenyl-1picylhydrazyl (DPPH), α-tocopherol, L-ascorbic acid, 2,2′-azino-bis (3-ethylbenzothiazoline-6-sulfonic acid) diammonium salt (ABTS), glycine hydrochloride (>99%), potassium chloride (puriss p.a. >99.5%), sodium chloride (puriss. p.a. >99.5%), sodium phosphate dibasic dihydrate, Tween® 80, Kollisolv® PEG E 400, potassium peroxodisulfate puriss (p.a., ACS reagent, >99%), fetal bovine serum, penicillin-streptomycin, trypsin-EDTA solution 0.25% (2.5 g porcine trypsin and 0.2 g EDTA), RPMI-1640 medium (with L-glutamine and sodium bicarbonate), and Cell counting kit-8 (CCK-8) were acquired from Sigma-Aldrich (St. Louis, MO, USA). Cibacron Brilliant Red 3B-A was obtained from Santa Cruz Biotechnology (Dallas, TX, USA). Lipopolysaccharide (from *Escherichia coli* 055: B5) sulfanilamide ≥98% and N- (1-naphthyl) ethylenediamine dihydrochloride ≥98% were purchased from Sigma Life Science Norway AS (Oslo, Norway). Blood agar plates, saline solution (0.85% w/v), and Muller-Hinton broth were provided by the University Hospital of North Norway (Tromsø, Norway). Ortho-phosphoric acid ≥85% was acquired from Kebo Lab Ab (Oslo, Norway). Acetonitrile, ethanol (96%), and trifluoroacetic acid were purchased from VWR Chemicals (Fontenay-sous-Bois, France). Dimethyl sulfoxide, cell culture reagent was obtained from MP Biomedicals (Santa Ana, CA, USA). *Staphylococcus aureus* (ATCC® BAA-1721™) MSSA476 was bought from LGC standards AB (Borås, Sweden). Murine macrophage RAW 264.7 cells were bought from ATCC (Manassas, VA, USA).

2.2. Nanoparticle preparation

2.2.1. Nanoparticle production

The LCNs were prepared based on the method described by Clementino and Sonvico [21,22], with minor modifications. The formulation was tailored *via* emulsification of an aqueous and an oil phase. The aqueous phase comprised 9.9 mL of ultrapure water, pre-filtered through a cellulose acetate membrane filter with a 0.45 µm pore size. To this, 100 µL of a 1% w/v chitosan solution (dissolved in 0.3 N HCl) was added under continuous magnetic stirring.

The oil phase consisted of 2 mL of a 2.5% w/v Lipoid S45 lecithin solution in ethanol, containing 35 mg each of Labrafac and Maisine, along with 30 mg of βCAR and 6.25 mg of CUR. An aliquot of 0.8 mL of the oil phase was then slowly injected into the aqueous phase under magnetic stirring at 200 rpm until complete homogenization was achieved.

The LCNs without CUR or βCAR (unloaded LCNs) were prepared using the same procedure, omitting the active compounds, while single-loaded LCNs were produced by excluding either CUR or βCAR from the oil phase.

2.3. Characterisation of nanoparticles

2.3.1. Nanoparticle size and zeta potential determination

The particle size and polydispersity index (PI) of the LCNs were determined using dynamic light scattering (DLS) with a Zetasizer Nano ZS Zen 3600 (Malvern Instruments Ltd., Malvern, UK). For size and PI measurements, 20 µL of the formulation was diluted in 2 mL of ultrapure water in a disposable polystyrene cuvette [23]. Zeta potential measurements were conducted by diluting the samples 1:100 in a 1 mM KCl solution, using a folded capillary cell (DTS1070). All measurements were performed in triplicate at 25 °C [24].

2.3.2. Separation, entrapment efficiency, and relative recovery

The entrapment efficiency (EE%) of CUR and βCAR in the LCNs was determined according to the method previously described by Clementino and Sonvico [21]. The EE% was calculated using the following equation (Equation 1):

$$EE\% = \frac{Total\ amount\ of\ CUR/\beta CAR - Amount\ of\ free\ CUR/\beta CAR}{Total\ amount\ of\ CUR/\beta CAR} \times 100\% \quad (1)$$

The relative recovery (RR%) was calculated using the following equation (Equation 2):

$$RR\% = \frac{Amount\ of\ entrapped\ CUR/\beta CAR + Amount\ of\ unentrapped\ CUR/\beta CAR}{Initial\ loaded\ amout\ of\ CUR/\beta CAR} \times 100\% \quad (2)$$

To determine the total compound content, 600 µL of the nanoparticle suspension was diluted in 5 mL of ethanol to disrupt the LCN matrix and release the encapsulated compounds. For the assessment of non-encapsulated compound, 3 mL of the nanoparticle suspension was centrifuged at 1500 × *g* for 15 min (Heraeus Biofuge

Stratos, Heraeus Instruments, Hanau, Germany). After centrifugation, the supernatant was removed, and any precipitated crystals were dissolved in 5 mL of acetonitrile.

Additionally, to quantify the soluble, non-encapsulated fraction, 500 µL of the supernatant was subjected to ultrafiltration using Vivaspin® centrifugal concentrators (MWCO 1,000,000 Da; Sartorius, Göttingen, Germany) at 1500 × *g* for 15 min (Heraeus Biofuge Stratos, Heraeus Instruments, Hanau, Germany). An aliquot of 20 µL from the ultrafiltrate was diluted in 1 mL of acetonitrile and analysed by high-performance liquid chromatography (HPLC).

Quantification of CUR and βCAR was performed using HPLC on a Waters e2795 Alliance HT system (Waters Corporation, Milford, MA, USA). Calibration curves for each compound were constructed before analysis, following the method described by Shah et al. with minor modifications [25].

Chromatographic separation was achieved using a reverse-phase C18 column (Symmetry®, 250 × 4.6 mm, 5 µm; Waters Corp.) operated under linear gradient elution. The mobile phase consisted of solvent A (water with 0.05% trifluoroacetic acid) and solvent B (acetonitrile with 0.05% trifluoroacetic acid). The gradient program was as follows: 0 min, 60% B; 10 min, 75% B; 15 min, 85% B; 25 min, 95% B; 30 min, 95% A; 35 min, return to initial conditions.

The flow rate was maintained at 1.0 mL/min, with an injection volume of 50 µL. The column oven temperature was set to 25 °C. Detection was carried out using a Waters 2489 UV/Visible detector (Waters Corp.), with monitoring at 210 nm for βCAR and 370 nm for CUR.

2.3.3. Determination of surface-available chitosan

The amount of surface-available chitosan on the LCNs was determined using a colorimetric dye-binding assay, as previously described by Andersen et al. and Muzzarelli with minor modifications [26,27].

A glycine buffer (pH 3.2) was prepared by dissolving 1.87 g of glycine and 1.46 g of NaCl in 250 mL of distilled water. An aliquot of 81 mL of this buffer was then diluted with 0.1 M HCl to a final volume of 100 mL. A dye solution was prepared by dissolving 150 mg of Cibacron Brilliant Red 3B-A in 100 mL of distilled water and subsequently diluting 5 mL of this solution to 100 mL using the prepared glycine buffer.

The LCNs were diluted 1:2 (v/v) with distilled water, after which 3 mL of the dye solution was added. The samples were incubated, and the absorbance was measured at 575 nm using a Spark Multimode Microplate Reader (Tecan, Männedorf, Switzerland).

The percentage of surface-available chitosan was calculated using the following equation (Equation 3):

$$Surface-available\ chitosan\,(\%) = \frac{C_s}{C_C} \times 100\% \tag{3}$$

where C_s is the concentration of chitosan detected on the surface, and C_c is the total chitosan concentration used during LCN preparation.

A calibration curve was established using a chitosan stock solution prepared by suspending 0.5 g of chitosan powder in 50 mL of distilled water with magnetic stirring

at room temperature for 30 min. Subsequently, 2 mL of glacial acetic acid (99.8%) and 50 mL of distilled water were added, resulting in a final chitosan concentration of 0.5 mg/mL. The standard curve was constructed using the following concentrations: 2.5, 5, 7.5, 10, 13.3, 16.6, 25, 33.3, and 41.6 µg/mL

2.3.4. Scanning electron microscopy

The morphology of the co-loaded LCNs was evaluated using a ZEISS SIGMA VP Field Emission Scanning Electron Microscope (SEM, Carl Zeiss, Oberkochen, Germany). Samples were diluted 1:5 in deionized water, and 10 µL of the suspension was deposited onto conductive carbon adhesive tape. After air drying for 24 h at room temperature, the samples were analysed at an accelerating voltage of 2 kV.

2.4. In vitro curcumin release

In vitro release studies were conducted using Franz diffusion cells (15 mm diameter, 12 mL receptor volume; PermeGear, Hellertown, PA, USA). The receptor medium consisted of a mixture of 20% ethanol, 10% polyethylene glycol (PEG) 400, 5% Tween® 80, and 65% phosphate-buffered saline (PBS) due to the poor aqueous solubility of the compound [28]. The PBS was prepared by dissolving NaCl (4 g), KCl (100 mg), Na_2HPO_4 (720 mg), and KH_2PO_4 (123 mg) in 500 mL of deionized water, followed by pH adjustment to 7.4. Sartolon® polyamide membranes (0.2 µm pore size; Sartorius Stedim Biotech GmbH, Göttingen, Germany) were cut to size and pre-conditioned in the receptor medium for 30 min before diffusion cell assembly.

During the experiment, the receptor chambers were filled with the pre-warmed medium and maintained at 32 °C using a circulating water bath, with magnetic stirring to ensure homogeneity. A total of 600 µL of each formulation was added to the donor chambers. A control solution containing free CUR and βCAR at equivalent concentrations was used for comparison.

Aliquots of 500 µL were collected from the receptor chambers at pre-determined time points (1, 2, 3, 4, 5, 6, 7, 8, and 24 h) and replaced with an equal volume of fresh medium. At the 24-h endpoint, the remaining receptor solution was collected, and the membranes were immersed in 5 mL of methanol to extract any retained CUR. Quantification of CUR in the receptor fluid and membrane extracts was performed spectrophotometrically at 370 nm using a Spark Multimode Microplate Reader (Tecan).

The Korsmeyer-Peppas model was applied to evaluate whether the release of the active compound was controlled by diffusion, polymer relaxation, or a combination of both, as described by Equation (4). In this model, M_t/M_∞ represents the fraction of the compound released at a given time t and is dimensionless. K_m is the release rate constant, reflecting the structural and geometric characteristics of the system, while n is the release exponent, which provides insight into the underlying mechanism of drug release [29].

$$M_t / M_\infty = Km \times n^t \tag{4}$$

Additionally, the flux (J) and apparent permeability (P_{app}) of the formulations was estimated to further characterize their release behaviour using Equations (5) and (6), respectively.

$$J = \frac{dQ}{dt \times A} \tag{5}$$

where dQ/dt is the slope of the cumulative amount of CUR permeated over time and A is the surface area of the membrane or barrier.

$$P_{app} = \frac{J}{C_0} \tag{6}$$

where J is the calculated flux and C_0 is the initial drug concentration in the donor compartment.

2.5. Radical scavenging assays

2.5.1. ABTS scavenging assay

The ABTS•$^+$ radical scavenging activity of CUR was evaluated according to the protocol described previously [30], with slight modifications. The ABTS•$^+$ radical cation was generated by mixing equal volumes (3 mL) of 7.4 mM ABTS stock solution and 2.6 mM potassium persulfate solution, followed by incubation in the dark at room temperature for 12–16 h. The resulting solution was diluted in ethanol (100 mL) before use.

To assess antioxidant activity, equal volumes (300 µL) of the ABTS•$^+$ solution and test samples, CUR at final concentrations of 5, 10, and 20 µg/mL, were mixed and incubated in the dark at room temperature for 30 min. As positive controls, vitamin C and vitamin E were included at the same concentrations. Absorbance was measured at 731 nm using a Spark Multimode Microplate Reader (Tecan).

The radical scavenging activity was calculated using the following equation (Equation 7):

$$Scavenging\ activity\,(\%) = \frac{A_{control} - A_{sample}}{A_{control}} \times 100\% \tag{7}$$

where $A_{control}$ is the absorbance of the DPPH solution without sample and A_{sample} is the absorbance in the presence of the test compound.

2.5.2. DPPH scavenging assay

The antioxidant properties of CUR were also evaluated using the 2,2-diphenyl-1-picrylhydrazyl (DPPH) radical scavenging assay, as described by Jøraholmen et al. with slight modifications [30]. The DPPH was prepared in ethanol at a final concentration of 60 µM. Test samples of CUR were diluted to final concentrations of 1, 5, 10, and 20 µg/mL. Parallel samples of vitamin C and vitamin E at the same concentrations were prepared and used as positive controls.

For each measurement, 300 µL of the sample solution was mixed with 300 µL of DPPH solution and incubated in the dark at room temperature for 30 min. The

reduction in absorbance, corresponding to scavenging of the DPPH radical, was measured at 519 nm using a Spark Multimode Microplate Reader (Tecan). All samples were analysed in triplicate. The radical scavenging activity was calculated as described in section 2.5.1.

2.5. Cell studies

2.5.1. Anti-inflammatory evaluation

The anti-inflammatory activity of the LCNs was evaluated using an NO inhibition assay in lipopolysaccharide (LPS)-induced RAW 264.7 macrophages, following a method described by Hemmingsen et al. [31]. Macrophages (5×10^5 cells/mL) were seeded in 24-well plates and cultured in RPMI-1640 medium supplemented with 10% fetal bovine serum (FBS) and 1% (v/v) penicillin-streptomycin and incubated for 24 h at 37 °C in a 5% CO_2 atmosphere. After incubation, the medium was replaced with fresh RPMI-1640 containing 1 µg/mL LPS to induce inflammation, and the cells were treated with 10 µL of either blank or co-loaded LCNs at three lipid concentrations: 1, 10, and 20 µg/mL. These corresponded to CUR concentrations of 0.12, 1.25, and 2.5 µg/mL, and βCAR concentrations of 0.5, 5.6, and 11.2 µg/mL, respectively.

Negative controls included untreated cells cultured in RPMI-1640 alone, while positive controls consisted of cells exposed to 1 µg/mL LPS without treatment. After 24 h of incubation, NO production was assessed by measuring nitrite levels in the culture supernatant using the Griess reagent (1:1 v/v; 2 g sulfanilamide and 200 mg N-(1-naphthyl) ethylenediamine dihydrochloride dissolved in 200 mL of 2.5% phosphoric acid). Absorbance was measured at 560 nm using a Spark Multimode Microplate Reader (Tecan). The percentage of NO inhibition was calculated by comparing treated samples to the LPS-induced positive control, which was considered 100% NO production.

2.5.2. Biocompatibility

The potential cytotoxicity of the LCNs was assessed using the Cell Counting Kit-8 (CCK-8), following the manufacturer's protocol as previously described by Hemmingsen et al. [31]. This colorimetric assay is based on the reduction of a tetrazolium salt by cellular dehydrogenases in viable cells to produce a water-soluble, orange-coloured formazan. The absorbance of the resulting solution, which is directly proportional to the number of metabolically active cells, was measured as an indicator of cell viability [32].

Murine RAW 264.7 macrophages were suspended in complete RPMI-1640 medium (supplemented with 10% FBS and 1% penicillin-streptomycin) at a concentration of 1×10^5 cells/mL. A volume of 90 µL of the cell suspension was seeded into each well of a 96-well plate and incubated for 24 h at 37 °C in a 5% CO_2 atmosphere to allow for cell adherence.

Following incubation, 10 µL of each test formulation was added to the wells. Treatments included: CUR-loaded LCNs, CUR and βCAR co-loaded LCNs, CUR dissolved in dimethyl sulfoxide (DMSO), and DMSO alone. The LCNs were tested at lipid concentrations of 1, 10, and 50 µg/mL. For each LCN treatment, a CUR concentration in the DMSO solution was prepared to correspond to the concentration of

CUR encapsulated in the corresponding LCN formulation. Specifically, for LCNs tested at lipid concentrations of 1, 10, and 50 µg/mL (corresponding to CUR concentrations of 0.12, 1.25, and 2.5 µg/mL, respectively), the free CUR in DMSO was adjusted to these same concentrations. This ensured a direct comparison of the effects of free *versus* encapsulated CUR at equivalent doses. Furthermore, DMSO alone at matching solvent concentrations was included to control for potential solvent toxicity. Untreated cells, receiving only pre-warmed complete medium, served as negative controls. Plates were incubated for an additional 24 h under the same conditions.

After treatment, 10 µL of CCK-8 reagent was added to each well, followed by a 4-h incubation at 37 °C in a 5% CO_2 atmosphere. Absorbance was then measured at 450 nm with a reference wavelength of 650 nm using a Spark Multimode Microplate Reader (Tecan).

2.6. Antimicrobial evaluation

The *in vitro* antimicrobial activity of the co-loaded and blank LCNs was evaluated following the protocol described by Balouiri et al. using a broth microdilution method [33]. Briefly, each test formulation (125 µL) was subjected to 2-fold serial dilution across eleven consecutive concentrations, with an untreated sample included as the negative control.

A bacterial suspension of *S. aureus* MSSA476 was prepared by adjusting turbidity to 0.5 McFarland standard in sterile saline solution (0.85% w/v), corresponding to ~1×10^8 colony forming units (CFU)/mL. This suspension was further diluted in Mueller–Hinton broth to achieve a final concentration of 1×10^6 CFU/mL. Then, 125 µL of the bacterial inoculum was added to each well containing the serial dilutions of the formulations. The plates were incubated at 37 °C for 24 h with shaking at 100 rpm.

After incubation, 20 µL from each well were transferred into the first row of a new 96-well plate pre-filled with 180 µL of PBS. A 10-fold serial dilution was then performed. Subsequently, 25 µL of each dilution was spotted on blood agar plates, allowed to dry, and incubated overnight at 37 °C.

The antimicrobial efficacy was assessed by comparing the number of surviving bacterial colonies in treated wells to the control well (without formulation), enabling quantification of bacterial inhibition.

2.7. Statistical analysis

In general, results are expressed as mean ± *SD*. Student's *t*-tests or one-way ANOVA with Tukey post-test were performed to evaluate significance ($p < 0.05$). All statistical analyses were performed in GraphPad Prism version 10.6.0 for Windows (GraphPad Software LLC, San Diego, CA, USA).

3. Results and discussions

3.1. Nanoparticle characterisation

Lecithin-chitosan nanoparticles (LCNs) have emerged as promising carriers for topical drug delivery due to their biocompatibility, bioadhesive properties, and ability to

enhance skin penetration [18,34,35]. In this study, LCNs were tailored to encapsulate βCAR and CUR, two relatively lipophilic compounds with known anti-inflammatory and antioxidant activities relevant to skin therapeutics. The βCAR was selected for its well-documented anti-inflammatory and antimicrobial properties, which complement CUR's biological activity. Moreover, its pronounced lipophilicity makes it particularly suitable for incorporation into LCNs, potentially affecting encapsulation, sustained release, and arrangement within the particles. The co-loading of these two natural compounds was also intended to explore potential additive or synergistic effects within a single delivery system. The effect of their incorporation on the structural features of the nanoparticles was evaluated through detailed characterization. Parameters such as particle size, PI, and zeta potential were measured for unloaded LCNs and those loaded with either or both compounds.

Comparing previously reported nanocarrier system with our study highlights the contribution of our co-loaded system. First, CUR-loaded nanostructured lipid carriers accelerated wound closure in full-thickness skin injuries, achieving 1.15–1.9-fold higher closure in the first week compared to CUR or control treatments [36]. Additionally, CUR-cyclodextrin hybrid nanoparticles exhibited strong anti-inflammatory, antioxidant, and broad-spectrum antibacterial effects, along with sustained release and enhanced fibroblast proliferation and migration *in vitro* [37]. Finally, CUR-loaded gold nanoparticles demonstrated superior antibacterial activity and faster wound healing in diabetic rat models compared to free CUR [38]. Separately, βCAR-loaded nanostructured lipid carriers improved skin retention and sustained release for topical applications [39]. Moreover, βCAR-loaded microemulsion-based hydrogels also displayed enhanced skin retention and anti-inflammatory effects compared to conventional gels, suggesting potential for improved topical treatment outcomes [40].

While these studies demonstrate the therapeutic potential of individually loaded CUR or βCAR nanocarriers, the co-loading of both compounds within a single LCN system is novel. The co-loaded LCNs combine the antimicrobial, anti-inflammatory, and antioxidative properties of CUR and βCAR, enabling the simultaneous targeting of multiple effects. This dual-loading strategy might potentially provide additive or synergistic effects that are not typically possible with single-compound carriers.

3.1.1. Nanoparticle characteristics

Table 1 presents the characteristics of the various LCNs, including unloaded, individually loaded, and co-loaded nanoparticles. Incorporation of active compounds, particularly CUR and βCAR, lead to a gradual decrease in particle size that was significant in all formulations except between the CUR-LCNs and the co-loaded LCNs, while the reduction in the magnitude of the positive surface potential is minor and not

Table 1. Size, PI, and zeta potential of all nanoparticle formulations.

	Size (nm)	PI[a]	Zeta potential (mV)
LCNs	236.0 ± 1.9	0.186 ± 0.002	34.9 ± 3.6
βCAR-LCNs	222.9 ± 2.9	0.187 ± 0.008	32.4 ± 0.9
CUR-LCNs	210.4 ± 3.0	0.176 ± 0.008	31.8 ± 2.0
Co-loaded-LCNs	208.7 ± 3.5	0.173 ± 0.007	31.2 ± 3.3

Results are expressed as means with their respective *SD*s ($n = 3$).
[a]Polydispersity index.

statistically significant. These changes are most pronounced in the co-loaded formulation, suggesting an additive effect of dual loading on nanoparticle structure. Despite the decrease in size, the PI remains relatively stable across all formulations, indicating uniform particle distribution. Particle sizes below 250–300 nm with a PI under 0.3 are considered favourable for topical skin delivery, facilitating close interaction with the *stratum corneum*, promoting passive diffusion, and enhancing retention within the superficial skin layers [41,42]. The particle size, PI, and zeta potential observed in this study are comparable to those reported in the literature. In particular, similar physicochemical characteristics have been documented by Clementino and Sonvico, as well as by Gerelli et al. and Şenyiğit et al. [21,35,43].

The EE% was consistently relatively high for both CUR and βCAR, indicating that LCNs provide a suitable lipophilic environment for their incorporation (Table 2). The co-loaded formulation further significantly improved encapsulation, suggesting complementary partitioning of the two compounds within the lipid matrix. Furthermore, the RR% revealed significant differences. Namely, CUR alone showed moderate recovery, but its stability markedly improved when co-loaded with βCAR, whereas βCAR recovery decreased slightly under the same conditions. This pattern suggests that the presence of βCAR might improve CUR stability, while CUR incorporation might in turn influence βCAR distribution within the lipid core. Overall, co-loading appears to improve CUR incorporation and recovery, while simultaneously slightly reduce βCAR recovery.

The SEM images of the co-loaded LCNs supported the findings obtained from DLS measurements (Figure 1). The nanoparticles appeared as near-spherical structures with relatively uniform morphology, consistent with the narrow size distribution indicated by the relatively low PI values. The observed particle sizes in the SEM micrographs aligned with the nanoparticle size measured by DLS, confirming the successful formation of nanoparticles. Together with the measured zeta potential and encapsulation efficiencies for both βCAR and CUR (Table 2), these results confirm the reproducibility and robust physicochemical profile of the developed LCNs. The near-spherical shape is advantageous for topical applications, as it can facilitate better skin contact and uniform spreading across the application site. Compared with the particles reported by Şenyiğit et al., which exhibited an even smoother and more well-defined surface [35], the present LCNs still demonstrated suitable characteristics for topical delivery. Given their suspension form, the nanoparticles would require incorporation into secondary delivery systems such as hydrogels, nanofiber scaffolds, or film-forming dressings for practical topical application [44–46].

Table 2. Entrapment of CUR and βCAR and relative recovery of all nanoparticle formulations.

	EE_{CUR}%[a]	$EE_{\beta CAR}$%[b]	RR_{CUR}%[c]	$RR_{\beta CAR}$%[d]
βCAR-LCNs	–	99.21 ± 0.16	–	61.24 ± 0.23
CUR-LCNs	95.30 ± 2.00	–	59.95 ± 6.39	–
Co-loaded-LCNs	99.99 ± 0.01*	99.94 ± 0.08*	85.40 ± 0.16*	55.67 ± 0.10*

Results are expressed as means with their respective *SD*s ($n = 3$).
*$p \leq 0.05$ compared to the relevant formulation, determined by Student's *t*-test.
[a]Entrapment efficiency (%) for curcumin.
[b]Entrapment efficiency (%) for β-caryophyllene.
[c]Relative recovery (%) for curcumin.
[d]Relative recovery (%) for β-caryophyllene.

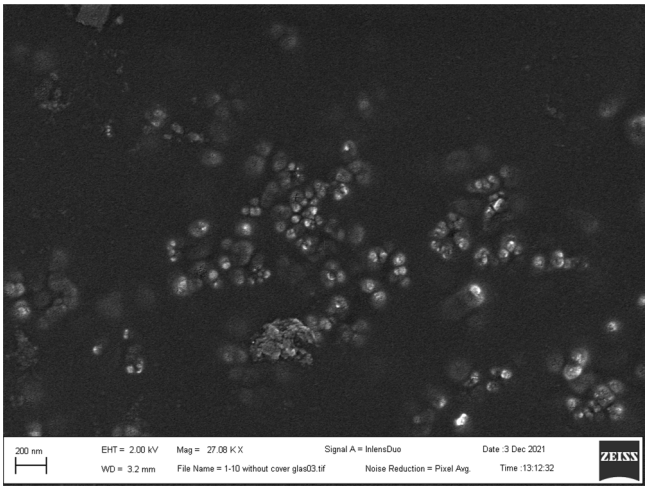


Figure 1. Scanning electron microscopy image of co-loaded lecithin-chitosan nanoparticles containing both curcumin and β-caryophyllene. Scale bar = 200 nm.

3.1.2. Surface-available chitosan

The quantification of surface-available chitosan revealed that ~22% (22.28 ± 0.75%) of the total chitosan content is exposed on the outer surface of the LCNs. This partial surface availability is consistent with the structural organization of the nanoparticles, where chitosan primarily forms the outer shell but might be partially embedded within the interfacial layer during self-assembly [22]. The presence of surface-available chitosan is particularly important for topical delivery, as it contributes to the cationic character of the nanoparticles, enhancing electrostatic interactions with the negatively charged skin and bacterial surfaces [47]. This interaction could promote closer contact with the *stratum corneum*, improve retention at the application site, and potentially facilitate accumulation in the skin. Moreover, surface-available chitosan could also influence the bioadhesive properties and biological activity of the formulation, including antimicrobial effects and modulation of skin barrier function [48–51]. Therefore, a surface-available fraction of about 22% could indicate a positive balance between structural stability and functional surface activity for skin-targeted applications. The CUR-LCNs could not be measured due to signal interference caused by CUR at the relevant wavelength. Notably, the surface-available chitosan fraction in these LCNs is far lower than that previously reported for chitosan-coated liposomes, which ranged from ~49 to 84% in different studies, highlighting a distinct structural arrangement in the current nanoparticle system and production procedure [26,52,53]. Although the surface chitosan fraction is relatively low, it reflects the outcome of optimizing the lecithin-to-chitosan ratio to achieve suitable particle size, PI, and zeta potential for dermal delivery. Higher surface availability of chitosan could potentially enhance bioadhesive interactions with the skin and bacterial membranes, thereby improving antimicrobial activity. Nevertheless, the current formulation demonstrated measurable antimicrobial effects and favourable skin retention, indicating that even partial surface exposure is sufficient to obtain activity.

3.2. In vitro CUR release

The *in vitro* release profiles of CUR over 24 h generally showed a gradual and sustained release across all formulations (Figure 2). While CUR-LCNs and co-loaded LCNs exhibited slightly higher cumulative permeation than free CUR, the differences were minimal, suggesting that encapsulation had only a modest effect on release under these conditions. The co-loaded LCNs showed a slightly lower release than CUR-LCNs ($p \geq 0.05$), conceivably reflecting the physical presence of βCAR within the nanoparticles, which might slightly influence the internal structure and lipophilic environment, thereby affecting CUR release. Overall, these findings indicate that LCN encapsulation maintains CUR availability over time but does not substantially alter its release profile compared to the unformulated compound. The release profile of βCAR was not investigated, as its extreme instability in the non-encapsulated state would likely compromise the reliability of the results.

In comparison with other CUR delivery systems, the release from the LCNs in the current study was relatively slow and limited. For instance, in another study, LCNs demonstrated a rapid burst and nearly complete release within 5 h [54], while solid lipid nanoparticles (SLNs) and SLN-loaded patches exhibited a sustained release pattern with ~55–60% of CUR released in the first 24 h [55]. In contrast, lipid-core nanocapsules showed only about 9% release after 48 h, indicating a much slower diffusion and release profile [56]. Almost all systems, including the present LCNs, displayed a controlled release phase; however, the total cumulative release of 17–19% observed for the LCNs in the current study suggests a more restrictive but prolonged delivery. Such a slower release profile might be beneficial in situations where prolonged local availability is desired, yet it also raises concerns about whether sufficient compound levels can be achieved within a relevant timeframe.

The Korsmeyer-Peppas model provides a robust description of the release behaviour for both LCN-based systems and the control (Table 3). This model accounts for both Fickian diffusion and non-Fickian (anomalous) transport mechanisms, making it particularly suitable for complex systems such as lipid- or polymer-based nanoparticles

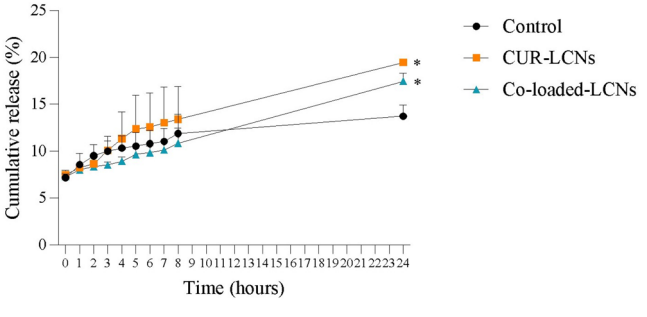


Figure 2. *In vitro* release profiles of curcumin from free curcumin solution (control), curcumin-loaded LCNs (CUR-LCNs), and co-loaded LCNs (containing both curcumin and β-caryophyllene) over 24 h at 32 °C, simulating skin temperature. The results are presented as means of the cumulative release (%) with their respective *SD*s ($n = 3$). *$p \leq 0.05$ compared to control at 24 h, determined by one-way ANOVA followed by Tukey's post-test.

Table 3. The Korsmeyer-Peppas model parameters.

Model	Parameter	Control	CUR-LCNs	Co-loaded-LCNs
Korsmeyer-Peppas model	K_m	0.0995	0.0560	0.0170
	n	0.416	0.742	1.048
	R^2	0.870	0.980	0.9995

Table 4. Normalized permeation parameters denoted as slope, flux, and apparent permeability.

	Control	CUR-LCNs	Co-loaded-LCNs
Slope (dQ/dt)	4.4109	5.9293	3.0272
Flux J	2.4920	3.3499	1.7103
R^2 (1–8 h)	0.9639	0.9561	0.9766
P_{app}	9.968×10^{-3}	1.340×10^{-2}	6.841×10^{-3}

P_{app}: apparent permeability.

that may undergo swelling, erosion, or structural relaxation during release [57]. The high correlation coefficients obtained from the Korsmeyer-Peppas fits indicate excellent agreement with the experimental data, particularly for the co-loaded LCNs, where the release approaches near zero-order kinetics. The model effectively depicts the multifaceted release behaviour of these formulations, reflecting their complex structural and release characteristics.

The Korsmeyer-Peppas model indicates that the CUR control follows Fickian diffusion, while CUR-LCNs exhibit anomalous transport involving potentially both diffusion and polymer relaxation, and co-loaded-LCNs display super case II transport potentially dominated by polymer swelling and erosion. The release rate constants decrease from CUR control to CUR-LCNs and co-loaded-LCNs, indicating slower release due to encapsulation and co-loading, possibly caused by structural rearrangements. The analysis suggests that LCN-based systems, particularly co-loaded-LCNs, achieve more sustained and complex release profiles compared to the primarily diffusion-controlled CUR control.

The permeability analysis (Table 4) based on the most linear region suggested that CUR-LCNs exhibited the highest slope, flux, and apparent permeability coefficient, indicating the most efficient diffusion across the membrane within the relevant time frame. The CUR control demonstrated moderate permeability, while the co-loaded LCNs showed the lowest flux and apparent permeability, suggesting a slower and more sustained release profile. These differences likely arise from variations in the structural arrangement and encapsulation, which influence release and diffusion behaviour. Based on the analysis, the CUR-LCNs seemingly provide enhanced permeability, whereas co-loaded LCNs might be better suited for controlled or prolonged release applications.

3.3. Radical scavenging

The antioxidative capacity of CUR was evaluated using ABTS and DPPH radical scavenging assays, with vitamins C and E serving as references (Figure 3). The use of two complementary assays was preferred as ABTS is water-soluble, representing a hydrophilic system, while DPPH is poorly water-soluble, representing a lipophilic environment. This dual approach allows assessment of CUR's radical scavenging

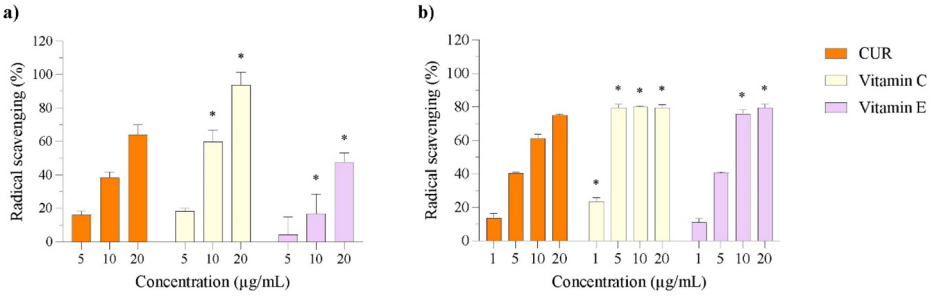


Figure 3. Radical scavenging activity of free curcumin (CUR), vitamin C, and vitamin E measured by ABTS (a) and DPPH (b) assays. The results are presented as means with their respective *SD*s ($n = 3$). *$p \leq 0.05$ compared to CUR, determined by one-way ANOVA followed by Tukey's post-test.

activity under different solubility conditions, which could be relevant for predicting its potential performance in complex biological or topical environments. In both assays, CUR exhibited concentration-dependent radical scavenging activity, showing slightly lower but overall comparable performance to vitamin E and vitamin C, two well-established lipophilic and hydrophilic antioxidants, respectively [58,59]. The selected CUR concentrations fall within the range typically assessed in antioxidative assays and are consistent with previously reported studies [60,61], where CUR demonstrated measurable radical-scavenging activity in the low µg/mL range. This range, therefore, captures both sub- and near-maximal antioxidative activity, allowing evaluation of concentration-dependent effects while maintaining comparable range with the literature. In the ABTS assay (Figure 3(a)), vitamin C demonstrated the strongest scavenging effect at the two highest concentrations, followed by CUR, while vitamin E showed the lowest activity. In the DPPH assay (Figure 3(b)), vitamin C consistently exhibited the strongest scavenging effect across all tested concentrations. At lower concentrations, CUR and vitamin E displayed similar activity; however, at higher concentrations, vitamin E slightly exceeded CUR in scavenging capacity. These results indicate that CUR possesses promising antioxidative properties, highlighting its potential as a multifunctional bioactive compound. Its comparable activity to vitamins C and E, which are widely used for skin protection, supports CUR's potential as a therapeutic agent against oxidative stress-related conditions.

Antioxidative activity is especially important in the topical treatment of chronic skin wounds, where prolonged inflammation and oxidative stress could significantly impair the healing process [62]. Excess ROSs in the wound environment could damage cellular structures, delay re-epithelialization, and worsen inflammation [5]. By neutralizing ROS, antioxidants help restore redox balance, promote tissue repair, and reduce inflammatory damage [63,64].

It is important to note that the antioxidative activity of co-loaded LCNs could not be directly measured in this study due to interference in the assay readings from the chitosan and pH conditions within the nanoparticle system. Despite this limitation, the free CUR measurements provide meaningful preliminary insight into its antioxidative potential, and previous reports suggest that incorporation of CUR into delivery systems could preserve or enhance its radical scavenging capacity [54,65].

3.4. Cell experiments

To evaluate the biocompatibility and therapeutic potential of the nanoparticle formulations, *in vitro* assays were conducted using mammalian cell models. These studies aimed to assess potential cytotoxicity, anti-inflammatory activity, and the impact on nitric oxide production in immune cells. Given the intended topical application for chronic wound treatment, it was essential to confirm that the LCNs were non-toxic at relevant concentrations and capable of modulating inflammatory responses associated with impaired healing.

3.4.1. Anti-inflammatory activity

The anti-inflammatory potential of the LCNs was assessed by measuring NO production in LPS-induced murine macrophages. Upon stimulation with LPS, macrophages produced high levels of NO. Treatment with unloaded LCNs at the highest tested concentration (20 µg/mL) resulted in a modest reduction in NO production (Figure 4), down to ~80% compared to the LPS control, suggesting a mild anti-inflammatory effect possibly attributable to the chitosan. In contrast, co-loaded LCNs containing both βCAR and CUR showed a dose-dependent and significantly stronger inhibition of NO production. At only 1 µg/mL, NO levels were reduced to about 70%, further decreasing to 54% at 10 µg/mL, and reaching 25% at 20 µg/mL. These results demonstrate a potential additive effect of the combination of compounds in suppressing macrophage-mediated inflammation. The selected concentration range covers commonly used doses for RAW 264.7 macrophages, allowing detection of concentration-dependent NO inhibition, consistent with previous studies using CUR-loaded lipid-based formulations [66–68].

This pronounced anti-inflammatory response is especially relevant in the topical treatment of chronic skin wounds, where persistent inflammation plays an important role in impaired healing. The ability of co-loaded LCNs to significantly reduce NO levels at low concentrations indicates their potential to modulate the inflammatory response effectively.

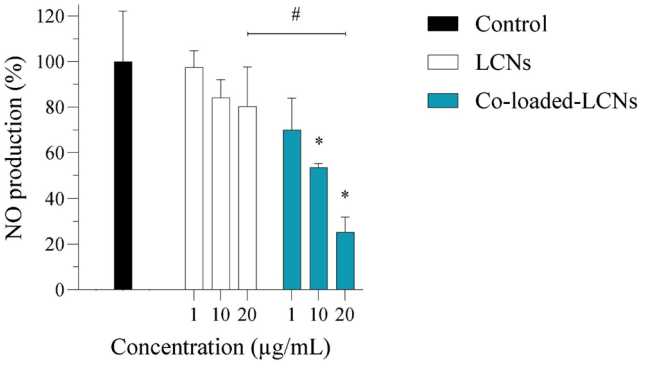


Figure 4. Effect of lecithin-chitosan nanoparticles (LCNs) and co-loaded LCNs on nitric oxide production in lipopolysaccharide-stimulated murine macrophages. Cells were treated with increasing lipid concentrations (1, 10, and 20 µg/mL) of each formulation. The results are presented as means with their respective *SD*s ($n = 3$). $^{*}p \leq 0.05$ compared to control, $^{\#}p \leq 0.05$ comparison between LCNs and co-loaded-LCNs, determined by one-way ANOVA followed by Tukey's post-test.

In comparison with a golden pompano head phospholipids and soybean lecithin (GPL) liposome system, which effectively inhibited LPS-induced NO, ROS, and cytokine production with superior efficacy observed for GPL-liposomes [69], the CUR-LCNs tailored in the current study demonstrated similar anti-inflammatory activities. In another study, a lecithin-based nanoemulsion of carnosic acid also enhanced NO inhibition relative to the free compound [70], further supporting the role of lipid-based carriers in improving the bioactivity. In contrast, CUR-loaded glucan nanoparticles showed weaker inhibition of NO than free CUR and, in some cases, promoted ROS production [71], emphasizing the importance of carrier design in achieving a favourable balance between efficacy and safety.

3.4.2. Biocompatibility

Toxicity assessments were conducted to evaluate the safety profile of CUR, including CUR dissolved in DMSO, DMSO alone, CUR-LCNs, and co-loaded LCNs at lipid concentrations of 1, 10, and 50 μg/mL or equivalent doses. The upper concentration in the anti-inflammatory assay was set at 20 μg/mL to evaluate therapeutic effects, while the toxicity assay included a higher concentration of 50 μg/mL to ensure that potential cytotoxic effects did not emerge just above the anti-inflammatory testing range. According to ISO standards, formulations maintaining cell viability above 80% are considered non-toxic [72]. Both CUR-LCNs and co-loaded LCNs demonstrated excellent biocompatibility across all tested concentrations, with no significant reduction in cell viability observed (Figure 5). Additionally, DMSO alone did not induce cytotoxicity, confirming that the solvent itself was not responsible for any adverse effects in the cell model.

In contrast, free CUR dissolved in DMSO exhibited pronounced cytotoxicity, reducing cell viability to about 14 and 18% at 10 and 50 μg/mL, respectively. This significant toxicity highlights the challenges associated with the direct use of CUR alone, potentially due to its poor solubility and potential for cellular membrane disruption at higher concentrations [73].

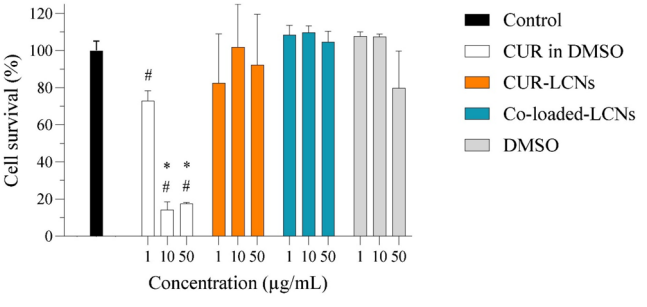


Figure 5. Cytotoxicity assessment of free curcumin in DMSO, DMSO alone, curcumin-loaded LCNs (CUR-LCNs), and co-loaded LCNs on mammalian cells. The LCN formulations were tested at lipid concentrations of 1, 10, and 50 μg/mL, corresponding to CUR concentrations of 0.12, 1.25, and 2.5 μg/mL, respectively. Free CUR in DMSO and DMSO alone were applied at the same CUR or solvent concentrations to allow direct comparison with the LCN formulations. The results are presented as means with their respective *SD*s ($n = 3$). $^{\#}p \leq 0.05$ compared to co-loaded-LCNs, $^{*}p \leq 0.05$ compared to control, determined by one-way ANOVA followed by Tukey's post-test.

Compared to previous studies, our findings are consistent with those of Valencia et al. Colaço et al. and Clementino et al. demonstrated that encapsulation substantially enhances the biocompatibility of CUR [65,71,74]. In line with Valencia et al., who reported that LCNs mitigated cytotoxicity in fibroblasts relative to free CUR [65], both CUR-LCNs and co-loaded LCNs in our study maintained RAW 264.7 macrophage viabilities above 80% across all tested concentrations, whereas free CUR exhibited pronounced cytotoxicity. Similarly, consistent with Colaço et al., glucan nanoparticles reduced CUR-associated cytotoxicity [71], and in agreement with Clementino et al., blank LCNs were non-toxic to THP-1 monocytic cells [74]. Our results are in contrast with the results of Guimarães et al., who reported that free CUR up to 10 µM did not affect macrophage viability [75].

3.5. Antimicrobial evaluation

The antimicrobial activity of the LCNs and the co-loaded LCNs was evaluated against *Staphylococcus aureus*, a common pathogen found in chronic wound infections [76]. Interestingly, unloaded LCNs exhibited a substantial antibacterial effect at a lipid concentration of 1 mg/mL, corresponding to CUR and βCAR concentrations of 125 and 560 µg/mL, for loaded LCNs, respectively, reducing *S. aureus* growth to ~3% relative to untreated controls (Figure 6). This pronounced antimicrobial activity could be attributed to the presence of chitosan, which is well known for its intrinsic bactericidal properties, including disruption of bacterial cell membranes and interference with the microbial envelope [47].

Nevertheless, the co-loaded LCNs, containing both βCAR and CUR, exhibited an even more pronounced antimicrobial effect at a lipid concentration of 0.5 mg/mL, reducing bacterial growth to ~0.2%. This significantly enhanced activity potentially

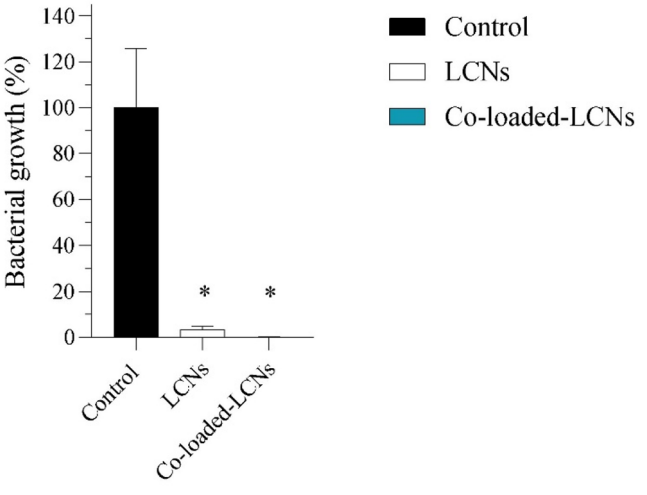


Figure 6. Evaluation of the antimicrobial properties of unloaded (LCNs, lipid concentration: 1 mg/mL) and co-loaded lecithin-chitosan nanoparticles (co-loaded-LCNs, lipid concentration: 0.5 mg/mL) against *Staphylococcus aureus*. The results are presented as means with their respective *SD*s ($n = 3$). *$p \leq 0.05$ compared to control, determined by one-way ANOVA followed by Tukey's post-test.

results from the combined antibacterial effects of CUR and βCAR, both of which have documented antimicrobial properties, as well as the potential interactions within the nanoparticle and chitosan's antimicrobial potential. This would confirm that the combined approach relying on the synergistic activities of individual components holds a promise, as would dressing.

The strong antimicrobial effect demonstrated by these nanoparticles is highly relevant for chronic wound management, where persistent bacterial colonization and infection are major obstacles to healing. Importantly, *S. aureus* infections often lead to biofilm formation, increased inflammation, and delayed tissue regeneration [77]. By reducing bacterial load, these LCNs could also potentially help reduce or disrupt biofilms, lower infection risk, and create a more favourable environment for wound repair. Future evaluation of their activity against gram-negative pathogens such as *Escherichia coli* and *Pseudomonas aeruginosa* would also be of interest, given the clinical significance of these bacteria in chronic wounds. Furthermore, the dual functionality of the co-loaded LCNs combining antimicrobial, anti-inflammatory, and antioxidant properties addresses multiple pathological factors simultaneously.

Previous studies have highlighted the significant antimicrobial properties of CUR. Tyagi et al. reported that CUR I exerts potent bactericidal activity against *S. aureus*, achieving complete killing at 100 μM even at high cell density, primarily through membrane disruption as shown by permeability assays and microscopy [78]. Furthermore, Adeyemi et al. reported that CUR exhibited strong antibacterial activity against *S. aureus* (minimum inhibitory concentration, MIC ≈ 600 μg/mL), inducing oxidative stress, lipid peroxidation, DNA fragmentation, and activation of the kynurenine pathway. These effects suggest that CUR's antimicrobial action involves oxidative damage leading to growth inhibition and cell death [79], while in photodynamic therapy, Imaizumi et al. found that CUR can induce bacterial cell wall damage under activating conditions [80].

Moreover, βCAR has also shown antimicrobial activity against *S. aureus*. Dahham et al. reported that βCAR exhibited strong antibacterial activity against *S. aureus*, with a low MIC of 3 μM [81]. Santos et al. demonstrated that βCAR exhibits strong antibacterial activity against *S. aureus*, with MIC values as low as 32 μg/mL. The study also showed that βCAR enhanced the activity of conventional antibiotics, such as norfloxacin and gentamicin, reducing their MICs against resistant *S. aureus* strains [82].

The antibacterial activity of the LCNs against *S. aureus* observed in this study aligns with prior studies demonstrating the efficacy of CUR-loaded and chitosan-based nanoparticles. Valencia et al. reported that LCNs containing CUR inhibited *S. aureus* growth at low concentrations [65]. This is also in line with Jia et al., who showed that lecithin-containing micelles enhanced bacterial uptake and disrupted cell membranes [83], the co-loaded LCNs in the current study could potentially benefit from a similar mechanism. Additionally, the results reported by Bahrani et al. confirm the intrinsic antibacterial potential of chitosan-lecithin hybrid nanoparticles against *S. aureus* [84]. Furthermore, Liu et al. reported that unloaded LCNs exhibited intrinsic antibacterial activity against *S. aureus*, producing inhibition zones of about 1.02 cm, indicating that the nanoparticle matrix itself can contribute to bacterial growth inhibition [17].

4. Conclusion

This study demonstrated the development and characterization of LCNs co-loaded with CUR and βCAR, tailored for the topical treatment of chronic skin wounds. The nanoparticles exhibited favourable properties, including size, low PI, and a stable surface charge, potentially making them suitable for dermal application. Biological evaluations suggested multifunctional therapeutic effects, with notable antioxidative, anti-inflammatory, and antimicrobial activities, while maintaining biocompatibility. Although these results indicate promise for co-delivery of CUR and βCAR, practical topical application will require formulation into sprays or incorporation into secondary delivery vehicles such as hydrogels or nanofiber scaffolds. Future studies should focus on *in vivo* validation of efficacy and safety, long-term stability, and formulation scalability to support clinical translation. These findings provide a foundation for the rational design of multifunctional nanocarrier-based topical treatments for chronic wounds.

Acknowledgements

We gratefully acknowledge Chitinor (Tromsø, Norway), Lipoid GmbH (Ludwigshafen, Germany), and Azelis (Herlev, Denmark) for kindly providing the chitosan, phospholipid, and Maisine® CC and Labrafac™ lipophile WL 1349 (Gattefossé), respectively, used in this study.

Disclosure statement

No potential conflict of interest was reported by the author(s).

Funding

No funding was received.

ORCID

Lisa Myrseth Hemmingsen http://orcid.org/0000-0003-0425-8829
Fabiola Guareschi http://orcid.org/0000-0001-9834-3279
Fabio Sonvico http://orcid.org/0000-0001-7372-1456
Nataša Škalko-Basnet http://orcid.org/0000-0002-4301-2840

Data availability statement

The data that support the findings of this study are available from the corresponding author, LMH, upon reasonable request.

References

[1] Rațiu S, Mariș MI, Furdui-Lința AV, et al. Oxidative stress in the pathophysiology of chronic venous disease: an overview. Antioxidants. 2025;14(8):989. doi: 10.3390/antiox14080989.

[2] Sharma A, Shankar R, Yadav AK, et al. Burden of Chronic Nonhealing Wounds: An Overview of the Worldwide Humanistic and Economic Burden to the Healthcare System. Int J Low Extrem Wounds. 2024;15347346241246339. doi: 10.1177/15347346241246339
[3] Martin P, Pardo-Pastor C, Jenkins RG, et al. Imperfect wound healing sets the stage for chronic diseases. Science. 2024;386(6726):eadp2974. doi: 10.1126/science.adp2974.
[4] Yadav JP, Singh AK, Grishina M, et al. Insights into the mechanisms of diabetic wounds: pathophysiology, molecular targets, and treatment strategies through conventional and alternative therapies. Inflammopharmacology. 2024;32(1):149–228. doi: 10.1007/s10787-023-01407-6.
[5] Xu Z, Liang B, Tian J, et al. Anti-inflammation biomaterial platforms for chronic wound healing. Biomater Sci. 2021;9(12):4388–4409. doi: 10.1039/D1BM00637A.
[6] Papadopoulou V, Sidders AE, Lu K-Y, et al. Overcoming biological barriers to improve treatment of a *Staphylococcus aureus* wound infection. Cell Chem Biol. 2023;30(5):513–526.e5. doi: 10.1016/j.chembiol.2023.04.009.
[7] Simonetti O, Marasca S, Candelora M, et al. Methicillin-resistant *Staphylococcus aureus* as a cause of chronic wound infections: alternative strategies for management. AIMS Microbiol. 2022;8(2):125–137. doi: 10.3934/microbiol.2022011.
[8] Monika P, Chandraprabha MN, Rangarajan A, et al. Challenges in healing wound: role of complementary and alternative medicine. Front Nutr. 2021;8(2021):791899. doi: 10.3389/fnut.2021.791899.
[9] Abd El-Hack ME, El-Saadony MT, Swelum AA, et al. Curcumin, the active substance of turmeric: its effects on health and ways to improve its bioavailability. J Sci Food Agric. 2021;101(14):5747–5762. doi: 10.1002/jsfa.11372.
[10] Ak T, Gülçin İ. Antioxidant and radical scavenging properties of curcumin. Chem Biol Interact. 2008;174(1):27–37. doi: 10.1016/j.cbi.2008.05.003.
[11] Friedrich RB, Kann B, Coradini K, et al. Skin penetration behavior of lipid-core nanocapsules for simultaneous delivery of resveratrol and curcumin. Eur J Pharm Sci. 2015;78:204–213. doi: 10.1016/j.ejps.2015.07.018.
[12] Gushiken LFS, Beserra FP, Hussni MF, et al. Beta-caryophyllene as an antioxidant, anti-inflammatory and re-epithelialization activities in a rat skin wound excision model. Oxid Med Cell Longev. 2022;2022(1):9004014. doi: 10.1155/2022/9004014.
[13] Koyama S, Purk A, Kaur M, et al. Beta-caryophyllene enhances wound healing through multiple routes. PLOS One. 2019;14(12):e0216104. doi: 10.1371/journal.pone.0216104.
[14] Nikoletic A, Natsaridis E, Flathmann T, et al. Soft nanocarriers as antimicrobial co-delivery systems to combat resistant infections. Adv Healthc Mater. 2025;14(21):e2404540. doi: 10.1002/adhm.202404540.
[15] Yang J, Jia C, Yang J. Designing nanoparticle-based drug delivery systems for precision medicine. Int J Med Sci. 2021;18(13):2943–2949. doi: 10.7150/ijms.60874.
[16] Jain AK, Jain S, Abourehab MAS, et al. An insight on topically applied formulations for management of various skin disorders. J Biomater Sci Polym Ed. 2022;33(18):2406–2432. doi: 10.1080/09205063.2022.2103625.
[17] Liu L, Ma Q, Wang S, et al. Efficient epidermal delivery of antibiotics by self-assembled lecithin/chitosan nanoparticles for enhanced therapy on epidermal bacterial infections. Int J Biol Macromol. 2022;218:568–579. doi: 10.1016/j.ijbiomac.2022.07.165.
[18] Rençber S, Bülbül EÖ, Senyigit ZA, et al. Bioadhesive nanoparticles as potent drug delivery carriers. Curr Med Chem. 2023;30(23):2604–2637. doi: 10.2174/0929867329666220613111635.
[19] Chuah L-H, Loo H-L, Goh CF, et al. Chitosan-based drug delivery systems for skin atopic dermatitis: recent advancements and patent trends. Drug Deliv Transl Res. 2023;13(5):1436–1455. doi: 10.1007/s13346-023-01307-w.
[20] Naveedunissa S, Meenalotchani R, Manisha M, et al. Advances in chitosan based nanocarriers for targetted wound healing therapies: a review. Carbohydr Polym Technol Appl. 2025;11:100891. doi: 10.1016/j.carpta.2025.100891.

[21] Clementino A, Sonvico F. Development and validation of a RP-HPLC method for the simultaneous detection and quantification of simvastatin's isoforms and coenzyme Q10 in lecithin/chitosan nanoparticles. J Pharm Biomed Anal. 2018;155:33–41. doi: 10.1016/j.jpba.2018.03.046.
[22] Sonvico F, Cagnani A, Rossi A, et al. Formation of self-organized nanoparticles by lecithin/chitosan ionic interaction. Int J Pharm. 2006;324(1):67–73. doi: 10.1016/j.ijpharm.2006.06.036.
[23] Mork S, Johannessen M, Škalko-Basnet N, et al. Chitosan and liposomal delivery systems for epicatechin or propyl gallate targeting localized treatment of vulvovaginal candidiasis. Int J Pharm. 2024;662:124489. doi: 10.1016/j.ijpharm.2024.124489.
[24] Thanh Nguyen H, Goycoolea FM. Chitosan/cyclodextrin/TPP nanoparticles loaded with quercetin as novel bacterial quorum sensing inhibitors. Molecules. 2017;22(11):1975. doi: 10.3390/molecules22111975.
[25] Shah S, Dhanani T, Sharma S, et al. Development and validation of a reversed phase high performance liquid chromatography-photodiode array detection method for simultaneous identification and quantification of coumarin, precocene-I, β-caryophyllene oxide, α-humulene, and β-caryophyllene in ageratum conyzoides extracts and essential oils from plants. J AOAC Int. 2020;103(3):857–864. doi: 10.1093/jaoacint/qsz038.
[26] Andersen T, Bleher S, Flaten GE, et al. Chitosan in mucoadhesive drug delivery: focus on local vaginal therapy. Mar Drugs. 2015;13(1):222–236. doi: 10.3390/md13010222.
[27] Muzzarelli RAA. Colorimetric determination of chitosan. Anal Biochem. 1998;260(2):255–257. doi: 10.1006/abio.1998.2705.
[28] Dong Y, Hengst L, Hunt R, et al. Evaluating drug distribution and release in ophthalmic emulsions: impact of release conditions. J Control Release. 2020;327:360–370. doi: 10.1016/j.jconrel.2020.08.020.
[29] Wu IY, Bala S, Škalko-Basnet N, et al. Interpreting non-linear drug diffusion data: utilizing Korsmeyer-Peppas model to study drug release from liposomes. Eur J Pharm Sci. 2019;138:105026. doi: 10.1016/j.ejps.2019.105026.
[30] Jøraholmen MW, Basnet P, Tostrup MJ, et al. Localized therapy of vaginal infections and inflammation: liposomes-in-hydrogel delivery system for polyphenols. Pharmaceutics. 2019;11(2):53. doi: 10.3390/pharmaceutics11020053.
[31] Hemmingsen LM, Panchai P, Julin K, et al. Chitosan-based delivery system enhances antimicrobial activity of chlorhexidine. Front Microbiol. 2022;13:1023083. doi: 10.3389/fmicb.2022.1023083.
[32] Cai L, Qin X, Xu Z, et al. Comparison of cytotoxicity evaluation of anticancer drugs between real-time cell analysis and CCK-8 method. ACS Omega. 2019;4(7):12036–12042. doi: 10.1021/acsomega.9b01142.
[33] Balouiri M, Sadiki M, Ibnsouda SK. Methods for *in vitro* evaluating antimicrobial activity: a review. J Pharm Anal. 2016;6(2):71–79. doi: 10.1016/j.jpha.2015.11.005.
[34] Khalil RM, El Arini SK, AbouSamra MM, et al. Development of lecithin/chitosan nanoparticles for promoting topical delivery of propranolol hydrochloride: design, optimization and *in-vivo* evaluation. J Pharm Sci. 2021;110(3):1337–1348. doi: 10.1016/j.xphs.2020.11.025.
[35] Şenyiğit T, Sonvico F, Rossi A, et al. *In vivo* assessment of clobetasol propionate-loaded lecithin-chitosan nanoparticles for skin delivery. Int J Mol Sci. 2016;18(1):32. doi: 10.3390/ijms18010032.
[36] Elkhateeb O, Badawy MEI, Tohamy HG, et al. Curcumin-infused nanostructured lipid carriers: a promising strategy for enhancing skin regeneration and combating microbial infection. BMC Vet Res. 2023;19(1):206. doi: 10.1186/s12917-023-03774-2.
[37] Abdel-Mageed HM, AbuelEzz NZ, Ali AA, et al. Newly designed curcumin-loaded hybrid nanoparticles: a multifunctional strategy for combating oxidative stress, inflammation, and infections to accelerate wound healing and tissue regeneration. BMC Biotechnol. 2025;25(1):49. doi: 10.1186/s12896-025-00989-z.
[38] Salama A, Elsherbiny N, Hetta HF, et al. Curcumin-loaded gold nanoparticles with enhanced antibacterial efficacy and wound healing properties in diabetic rats. Int J Pharm. 2024;666:124761. doi: 10.1016/j.ijpharm.2024.124761.

[39] Ghazwani M, Hani U, Alqarni MH, et al. Beta caryophyllene-loaded nanostructured lipid carriers for topical management of skin disorders: statistical optimization, *in vitro* and dermatokinetic evaluation. Gels. 2023;9(7):550. doi: 10.3390/gels9070550.
[40] Alharthi S, Ziora ZM, Mustafa G, et al. β-caryophyllene-loaded microemulsion-based topical hydrogel: a promising carrier to enhance the analgesic and anti-inflammatory outcomes. Gels. 2023;9(8):634. doi: 10.3390/gels9080634.
[41] Danaei M, Dehghankhold M, Ataei S, et al. Impact of particle size and polydispersity index on the clinical applications of lipidic nanocarrier systems. Pharmaceutics. 2018;10(2):57. doi: 10.3390/pharmaceutics10020057.
[42] Du Plessis J, Ramachandran C, Weiner N, et al. The influence of particle size of liposomes on the deposition of drug into skin. Int J Pharm. 1994;103(3):277–282. doi: 10.1016/0378-5173(94)90178-3.
[43] Gerelli Y, Di Bari MT, Deriu A, et al. Structure and organization of phospholipid/polysaccharide nanoparticles. J Phys: condens Matter. 2008;20(10):104211. doi: 10.1088/0953-8984/20/10/104211.
[44] Hemmingsen LM, Giordani B, Pettersen AK, et al. Liposomes-in-chitosan hydrogel boosts potential of chlorhexidine in biofilm eradication *in vitro*. Carbohydr Polym. 2021;262:117939. doi: 10.1016/j.carbpol.2021.117939.
[45] Lapmanee S, Bhubhanil S, Charoenphon N, et al. Cannabidiol-loaded lipid nanoparticles incorporated in polyvinyl alcohol and sodium alginate hydrogel scaffold for enhancing cell migration and accelerating wound healing. Gels. 2024;10(12):843. doi: 10.3390/gels10120843.
[46] Vedovatto S, Facchini JC, Batista RK, et al. Development of chitosan, gelatin and liposome film and analysis of its biocompatibility *in vitro*. Int J Biol Macromol. 2020;160:750–757. doi: 10.1016/j.ijbiomac.2020.05.229.
[47] Matica MA, Aachmann FL, Tøndervik A, et al. Chitosan as a wound dressing starting material: antimicrobial properties and mode of action. Int J Mol Sci. 2019;20(23):5889. doi: 10.3390/ijms20235889.
[48] Jøraholmen MW, Bhargava A, Julin K, et al. The antimicrobial properties of chitosan can be tailored by formulation. Mar Drugs. 2020;18(2):96. doi: 10.3390/md18020096.
[49] Lu T, Sun M, Zhou Y, et al. Self-powered chitosan/graphene oxide hydrogel band-aids with bioadhesion for promoting infected wounds healing. Int J Biol Macromol. 2024;283(Pt 2):137374. doi: 10.1016/j.ijbiomac.2024.137374.
[50] Song Y, Liu C, Xu X, et al. Chitosan-based multifunctional hydrogel with bio-adhesion and antioxidant properties for efficient wound hemostasis. Colloids Surf B Biointerfaces. 2024;234:113697. doi: 10.1016/j.colsurfb.2023.113697.
[51] Zamani S, Ehterami A, Vaez A, et al. Natural and synthetic polymers in burn wound healing. J Biomater Sci Polym Ed. 2025:1–66. doi: 10.1080/09205063.2025.2523505.
[52] Hemmingsen LM, Julin K, Ahsan L, et al. Chitosomes-in-chitosan hydrogel for acute skin injuries: prevention and infection control. Mar Drugs. 2021;19(5):269. doi: 10.3390/md19050269.
[53] Jøraholmen MW, Škalko-Basnet N, Acharya G, et al. Resveratrol-loaded liposomes for topical treatment of the vaginal inflammation and infections. Eur J Pharm Sci. 2015;79:112–121. doi: 10.1016/j.ejps.2015.09.007.
[54] Yu F, Luo H, Wang Y, et al. Preparation of curcumin-loaded chitosan/lecithin nanoparticles with increased anti-oxidant activity and *in vivo* bioavailability. Int J Biol Macromol. 2024;281(Pt 4):136659. doi: 10.1016/j.ijbiomac.2024.136659.
[55] Sabir F, Qindeel M, Rehman AU, et al. An efficient approach for development and optimisation of curcumin-loaded solid lipid nanoparticles' patch for transdermal delivery. J Microencapsul. 2021;38(4):233–248. doi: 10.1080/02652048.2021.1899321.
[56] Ortega A, da Silva AB, da Costa LM, et al. Thermosensitive and mucoadhesive hydrogel containing curcumin-loaded lipid-core nanocapsules coated with chitosan for the treatment of oral squamous cell carcinoma. Drug Deliv Transl Res. 2023;13(2):642–657. doi: 10.1007/s13346-022-01227-1.

[57] Fosca M, Rau JV, Uskoković V. Factors influencing the drug release from calcium phosphate cements. Bioact Mater. 2022;7:341–363. doi: 10.1016/j.bioactmat.2021.05.032.
[58] Blaner WS, Shmarakov IO, Traber MG. Vitamin A and vitamin E: will the real antioxidant please stand up? Annu Rev Nutr. 2021;41(1):105–131. doi: 10.1146/annurev-nutr-082018-124228.
[59] Fang Y-Z, Yang S, Wu G. Free radicals, antioxidants, and nutrition. Nutrition. 2002;18(10):872–879. doi: 10.1016/S0899-9007(02)00916-4.
[60] Choudhury AK, Raja S, Mahapatra S, et al. Synthesis and evaluation of the anti-oxidant capacity of curcumin glucuronides, the major curcumin metabolites. Antioxidants. 2015;4(4):750–767. doi: 10.3390/antiox4040750.
[61] Lee KJ, Oh YC, Cho WK, et al. Antioxidant and anti-inflammatory activity determination of one hundred kinds of pure chemical compounds using offline and online screening HPLC assay. Evid Based Complement Alternat Med. 2015;2015(1):165457. doi: 10.1155/2015/165457.
[62] Comino-Sanz IM, López-Franco MD, Castro B, et al. The role of antioxidants on wound healing: a review of the current evidence. J Clin Med. 2021;10(16):3558. doi: 10.3390/jcm10163558.
[63] He L, He T, Farrar S, et al. Antioxidants maintain cellular redox homeostasis by elimination of reactive oxygen species. Cell Physiol Biochem. 2017;44(2):532–553. doi: 10.1159/000485089.
[64] Ukaegbu K, Allen E, Svoboda KKH. Reactive oxygen species and antioxidants in wound healing: mechanisms and therapeutic potential. Int Wound J. 2025;22(5):e70330. doi: 10.1111/iwj.70330.
[65] Valencia MS, Silva Júnior MFd, Xavier-Júnior FH, et al. Characterization of curcumin-loaded lecithin-chitosan bioactive nanoparticles. Carbohydr Polym Technol Appl. 2021;2:100119. doi: 10.1016/j.carpta.2021.100119.
[66] Basnet P, Hussain H, Tho I, et al. Liposomal delivery system enhances anti-inflammatory properties of curcumin. J Pharm Sci. 2012;101(2):598–609. doi: 10.1002/jps.22785.
[67] Braido B, Rukavina Z, Grimstad Ø, et al. Liposomes-in-hydrogel for topical drug delivery: mechanical, kinetic, and biological insights. J Drug Deliv Sci Technol. 2025;113:107380. doi: 10.1016/j.jddst.2025.107380.
[68] Ternullo S, Gagnat E, Julin K, et al. Liposomes augment biological benefits of curcumin for multitargeted skin therapy. Eur J Pharm Biopharm. 2019;144:154–164. doi: 10.1016/j.ejpb.2019.09.016.
[69] Gao X, Yi X, Liu Z, et al. Comparative study on curcumin loaded in golden pompano (*Trachinotus blochii*) head phospholipid and soybean lecithin liposomes: preparation, characteristics and anti-inflammatory properties. Molecules. 2021;26(8):2328. doi: 10.3390/molecules26082328.
[70] Zheng H, Li J, Ning F, et al. Improving *in vitro* bioaccessibility and bioactivity of carnosic acid using a lecithin-based nanoemulsion system. Food Funct. 2021;12(4):1558–1568. doi: 10.1039/D0FO02636K.
[71] Colaço M, Roquito T, Costa JP, et al. The effect of curcumin-loaded glucan nanoparticles on immune cells: size as a critical quality attribute. Pharmaceutics. 2023;15(2):623. doi: 10.3390/pharmaceutics15020623.
[72] ISO. ISO, 10993-5:2009 biological evaluation of medical devices. Part 5: tests for *in vitro* cytotoxicity. Geneva: International Organization for Standardization-ISO; 2009.
[73] Kreczmer B, Dyba B, Barbasz A, et al. Curcumin's membrane localization and disruptive effects on cellular processes—insights from neuroblastoma, leukemic cells, and Langmuir monolayers. Sci Rep. 2024;14(1):16636. doi: 10.1038/s41598-024-67713-3.
[74] Clementino AR, Marchi C, Pozzoli M, et al. Anti-inflammatory properties of statin-loaded biodegradable lecithin/chitosan nanoparticles: a step toward nose-to-brain treatment of neurodegenerative diseases. Front Pharmacol. 2021;12(2021):716380. doi: 10.3389/fphar.2021.716380.

[75] Guimarães MR, Leite FRM, Spolidorio LC, et al. Curcumin abrogates LPS-induced pro-inflammatory cytokines in RAW 264.7 macrophages. Evidence for novel mechanisms involving SOCS-1, -3 and p38 MAPK. Arch Oral Biol. 2013;58(10):1309–1317. doi: 10.1016/j.archoralbio.2013.07.005.

[76] Del Giudice P. Skin infections caused by *Staphylococcus aureus*. Acta Derm Venereol. 2020;100(9):adv00110. doi: 10.2340/00015555-3466.

[77] Serra R, Grande R, Butrico L, et al. Chronic wound infections: the role of *Pseudomonas aeruginosa* and *Staphylococcus aureus*. Expert Rev Anti Infect Ther. 2015;13(5):605–613. doi: 10.1586/14787210.2015.1023291. [25746414]

[78] Tyagi P, Singh M, Kumari H, et al. Bactericidal activity of curcumin I is associated with damaging of bacterial membrane. PLOS One. 2015;10(3):e0121313. doi: 10.1371/journal.pone.0121313.

[79] Adeyemi OS, Obeme-Imom JI, Akpor BO, et al. Altered redox status, DNA damage and modulation of L-tryptophan metabolism contribute to antimicrobial action of curcumin. Heliyon. 2020;6(3):e03495. doi: 10.1016/j.heliyon.2020.e03495.

[80] Imaizumi U, Inaba K, Kurahashi A, et al. Effectiveness of curcumin-based antimicrobial photodynamic therapy against *Staphylococcus aureus*. J Oral Sci. 2023;65(4):270–274. doi: 10.2334/josnusd.23-0183.

[81] Dahham SS, Tabana YM, Iqbal MA, et al. The anticancer, antioxidant and antimicrobial properties of the sesquiterpene β-caryophyllene from the essential oil of *Aquilaria crassna*. Molecules. 2015;20(7):11808–11829. doi: 10.3390/molecules200711808.

[82] Santos EL, Freitas PR, Araújo ACJ, et al. Enhanced antibacterial effect of antibiotics by the essential oil of *Aloysia gratissima* (Gillies & Hook.) Tronc. and its major constituent beta-caryophyllene. Phytomed Plus. 2021;1(4):100100. doi: 10.1016/j.phyplu.2021.100100.

[83] Jia Y, Li Y, Wang M, et al. Lecithin-based mixed polymeric micelles for activity improvement of curcumin against *Staphylococcus aureus*. J Biomater Sci Polym Ed. 2025;36(5):587–604. doi: 10.1080/09205063.2024.2421089.

[84] Bahrani HMH, Ghobeh M, Homayouni Tabrizi M. The anticancer, anti-oxidant, and antibacterial activities of chitosan-lecithin-coated parthenolide/tyrosol hybrid nanoparticles. J Biomater Sci Polym Ed. 2023;34(11):1603–1617. doi: 10.1080/09205063.2023.2177473.